Demonstration of in-service wavelength division multiplexing optical-signal-to-noise ratio performance monitoring and operating guidelines for coherent data channels with different modulation formats and various baud rates

Mohammad Reza Chitgarha,[1,]* Salman Khaleghi,[1] Wajih Daab,[1] Ahmed Almaiman,[1]
Morteza Ziyadi,[1] Amirhossein Mohajerin-Ariaei,[1] Devora Rogawski,[1] Moshe Tur,[2]
Joseph D. Touch,[3] Vijay Vusirikala,[4] Wendy Zhao,[4] and Alan E. Willner[1]

[1]*Department of Electrical Engineering, University of Southern California, Los Angeles, California 90089, USA*

[2]*School of Electrical Engineering, Tel Aviv University, Ramat Aviv 69978, Israel*

[3]*Information Sciences Institute, University of Southern California, 4676 Admiralty Way, Marina del Rey, California 90292, USA*

[4]*Google Inc., 1600 Amphitheatre Parkway, Mountain View, California 94043, USA*

*Corresponding author: chitgarh@usc.edu

We demonstrated a delay-line interferometer (DLI)-based, optical-signal-to-noise ratio (OSNR) monitoring scheme of 100 Gbit/s polarization multiplexed quadrature-phase-shift-keying (PM-QPSK) four-channel WDM at 50-GHz International Telecommunication Union (ITU) grid with <0.5 dB error for signals with up to 26 dB of actual OSNR. We also demonstrated data format transparency and baud rate tunability of the OSNR monitor by measuring the OSNR for a 200 Gbit/s PM-16-QAM (25-Gbaud) signal and a 200 Gbit/s PM-QPSK (50-Gbaud) signal. We also explored and studied different monitor parameters, including the shape of the filter spectrum, the bandwidth of the filter, DLI delay, and DLI phase-detuning to determine the design guidelines for a desired level of accuracy for the OSNR monitor in an optical network.   © 2014 Optical Society of America

OCIS codes: (060.2360) Fiber optics links and subsystems; (060.4370) Nonlinear optics, fibers; (190.4223) Nonlinear wave mixing.

http://dx.doi.org/10.1364/OL.39.001605

Optical performance monitoring has gained much interest for helping maintain proper system operation in optical communication networks [1]. One of the most basic parameters to be measured at various points in a network is the optical signal-to-noise ratio (OSNR), which can decrease due to amplified spontaneous-emission (ASE) noise induced by cascaded erbium-doped fiber amplifiers (EDFAs) along the optical link [2–6]. It is important to maintain a high OSNR that is above the critical limit; otherwise data cannot be recovered, and the link will be considered to be "down."

An OSNR monitor should efficiently and accurately measure the in-channel-band OSNR, be cost effective, support integration with minimum complexity, and support ubiquitous deployment throughout the optical network. A key feature of such an OSNR is data format and symbol rate transparency.

A common technique for the in-band OSNR monitoring measures out-of-band noise and utilizes linear interpolation to estimate the in-band noise. In high-speed ROADM-based optical networks, each channel may traverse different optical filters and/or amplifiers, so the out-of-band noise gives no indication of in-channel-band noise and thus this method is inaccurate [2,3].

Another method to measure the in-band OSNR is polarization-nulling, which relies on the different polarization properties of the signal and ASE noise [7–11]. In this technique, the received signal passes through a polarization beam splitter in which one polarization consists only of the signal, and the other includes only ASE noise. The

accuracy of this method can be significantly degraded due to polarization-mode dispersion (PMD) and polarization-dependent loss (PDL) in the optical link, and it is not applicable for pol-muxed signals in which both polarization states are occupied by two polarized signals.

Here, we explore an OSNR monitor that relies on delay-line interferometry, which holds promise for achieving many of the desired characteristics by exploiting the difference between signal and noise coherence [2,12–15]. This monitor measures the optical power of the constructive and destructive output ports using simple, low-speed photodiodes in order to determine the power associated with the signal and the noise. To demonstrate its utility, we need to explore its ability to measure high-bit-rate, pol-muxed quadrature-phase-shift-keying (QPSK) and quadrature-amplitude modulation (QAM) data in a WDM system, and we need to determine important design guidelines and the level of accuracy for practical deployment.

This Letter demonstrates and provides design guidelines for a DLI-based OSNR performance monitor using 200 Gbit/s pol-muxed 16-QAM and 100 Gbit/s pol-muxed QPSK in both single and WDM data channels. An error of <0.5 dB in OSNR measurement was achieved for signals with <26 dB of actual OSNR. We also explored and studied different monitor parameters to determine the design guidelines for a desired level for the accuracy of a DLI-based, OSNR monitor in a network.

Figure 1 shows the basic design of a DLI-based, OSNR monitor for a WDM optical network. Inline EDFAs are shown as they would be used in a real network, and these
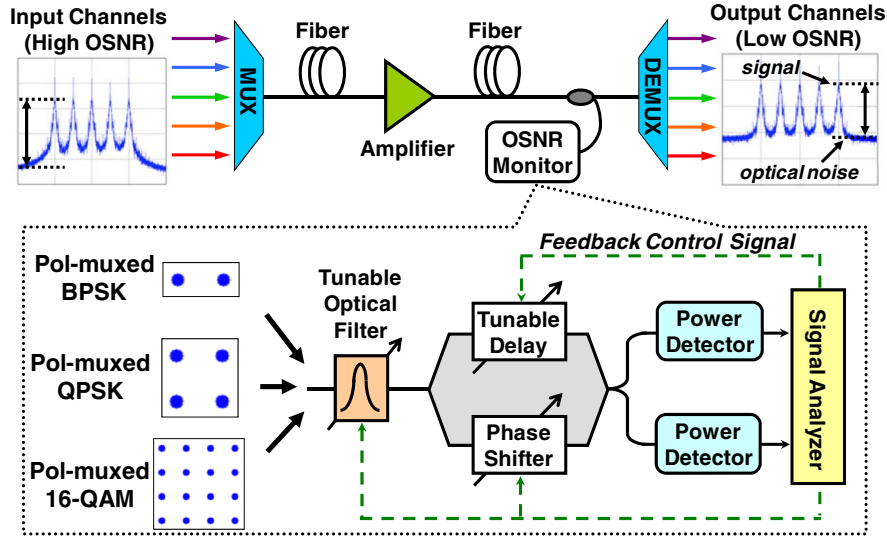
Fig. 1. Conceptual block diagram of the OSNR monitor for WDM channels using a delay-line interferometer.

degrade the quality of optical channels by decreasing the OSNR value. The OSNR monitor consists of an optical, tunable, bandpass filter (BPF), a Mach–Zehnder-based DLI, and two optical power meters.

For the OSNR calculation, first the OSNR monitor is calibrated at initialization to measure the signal distribution ratio (α) and the noise distribution ratio (β) at the DLI outputs. α is the ratio of constructive power to destructive power when the signal is set to the maximum OSNR (>30 dB), whereas β is the same ration when only noise is transmitted through the link. Then, the calibration parameters can be used to calculate the OSNR for the signal with an arbitrary amount of noise, due to the superposition property of the monitor components. Therefore, if P_{Const}, P_{Dest}, P_{Sig}, and P_{Noise} are the constructive power, the destructive power, the signal power, and the noise power, respectively, the following equations can be used to derive the OSNR:

$$P_{Const} = \frac{\alpha}{\alpha + 1} P_{Sig} + \frac{\beta}{\beta + 1} P_{Noise} \qquad (1)$$

$$P_{Dest} = \frac{1}{\alpha + 1} P_{Sig} + \frac{1}{\beta + 1} P_{Noise} \qquad (2)$$

$$\frac{P_{Sig}}{P_{Noise}} = \frac{\alpha + 1}{\beta + 1} \cdot \frac{P_{Const} - \beta P_{Dest}}{\alpha P_{Dest} - P_{Const}}. \qquad (3)$$

The standard OSNR value is

$$\text{OSNR(dB)} \triangleq 10 \log_{10}\left(\frac{P_{Sig}}{P_{Noise}} \cdot \frac{\text{NEB}}{0.1 \text{ nm}} \right), \qquad (4)$$

where NEB is the noise equivalent bandwidth of the filter. In this method, the transmitter parameters (e.g., bias and extinction ratio) might vary α and decrease the accuracy [2,14–16].

Figure 2 shows the OSNR monitoring setup. Four CW lasers at wavelengths, λ_{S1-4}, of 1549.72, 1550.12, 1550.52, and 1550.92 nm (channels 54, 55, 56, and 57 in the

50-GHz ITU grid) are coupled and sent into a pair of Mach–Zehnder modulators (MZMs) driven by 10, 25, or 50 Gbit/s pseudo-random bit sequences (PRBSs) $2^{31} - 1$ to generate four consecutive binary-phase-shift-keying (BPSK) or QPSK signals. These signals also can be passed through a 16-QAM emulator to generate 16-QAM signals at the same baud rates. Then, the single-polarization data path was split, delayed, and combined in a polarization beam combiner (PBC) to emulate a four-channel, pol-muxed, WDM, optical link. Then, this WDM link was passed through a tunable attenuator, coupled with a tunable output ASE noise source, and sent to the OSNR monitor. In the OSNR monitor, the WDM channels were filtered using a tunable optical filter with ~0.3 nm bandwidth to select the desired channel, which was then sent to the DLI after tapping 10% of the signal power to measure the actual OSNR value. Two optical power meters with 0.5% accuracy and 0.01 dB resolution were used to measure the optical power at the DLI output ports. During each experimental measurement, in order to align the DLI to the channel being tested, the DLI voltage was tuned so that the power ratio between constructive and destructive ports was maximized.

The design parameters for the OSNR monitor include the bandwidth of the filter (Δf), the profile of the filter,
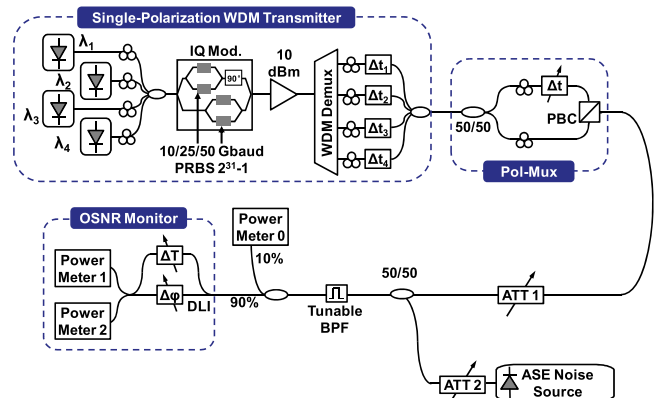
Fig. 2. Experimental setup for OSNR monitoring of pol-muxed WDM channels.

and the delay of DLI (ΔT). Figure 3 shows the simulation results for the accuracy of the OSNR monitor using a filter with different spectral shapes and bandwidths. Figures 3(a) and 3(b) compare the performance of the OSNR monitor for Gaussian, Lorentzian, and raised-cosine filters in simulations of both a single channel and a WDM system. In this configuration, the bandwidth and center frequency of all the filters were set to 35-GHz and 1550.12 nm, respectively, and the DLI delay was tuned to 10 ps. As shown, the Lorentzian filter resulted in the minimum error in the single-channel simulation, whereas a Gaussian filter had better performance for the WDM system. We believe the difference in the OSNR performance was due to the difference in roll-off factors in these three filters. Although the low roll-off factor in the Lorentzian filter decreased the error in the OSNR measurement in the single-channel simulation by increasing the difference between the signal and the noise coherence, it maximized the negative effects of the leaked neighboring channels in the WDM system. Figure 3(c) shows the accuracy of the OSNR monitor for the same types of filters with a different 3 dB bandwidth. In this simulation of the WDM system, the emulated OSNR was fixed at ~19 dB, the delay of the DLI was set to 10 ps, and the filter center wavelength was set to 1550.12 nm. As shown, although the minimum errors for Gaussian and raised-cosine filters occurred at ~25 and 30 GHz, respectively, the error associated with the Lorentzian filter was a minimum at the lowest bandwidth (i.e., 10 GHz) due to the importance of neighboring channel effects.

Figure 4(a) shows the accuracy of the proposed scheme for OSNR monitoring for DLIs with different delays for three levels of OSNR, i.e., low (10 dB), medium (15 dB), and high (20 dB). In this simulation, a

single-channel, 100 Gbit/s PM-QPSK, a Lorentzian filter with bandwidth of ~35 GHz, and a DLI with tunable delay were used. The results demonstrated that the error level increased for higher delays, which we believe was because the larger DLI FSR resulted in a greater difference between the signal and the noise coherence.

In Fig. 4(b), the actual OSNR was fixed at 20 dB, the FSR of the DLI was fixed at 100-GHz, and a Gaussian filter with a 35-GHZ bandwidth with a center wavelength of 1550.12 nm was used to measure the OSNR error (for the same levels of the actual OSNR) in both the simulations and the experiments for different DLI phase detunings. As shown, even a 20% detuning of the DLI phase (e.g., due to the inaccuracy of the applied voltage) resulted in ~1.5 dB of error in OSNR measurement for the actual 20-dB OSNR. In Fig. 4(c), an error margin of 18° (10%) was assumed for the DLI phase drift, and the total error of the OSNR measurement is depicted for different DLI delay values. This phase fluctuation can be caused by temperature changes in the experimental environment. This figure shows the simulation and experimental results using Gaussian and Lorentzian filters with a 35-GHz bandwidth, a tunable DLI, and the same three levels of OSNR (i.e., 10, 15, and 20 dB). We concluded that the optimum value for DLI delay was between 6 and 10 ps (~15–25% of the symbol time) for 100 Gbit/s PM-QPSK signals, for either Lorentzian or Gaussian filter shapes.

According to the simulation and experimental results on different parameters of the OSNR monitor, we concluded that accurate OSNR monitoring in an optical network requires consideration of the following design rules and guidelines. First, for monitoring a specific channel, the center frequency of the BPF filter needs to be
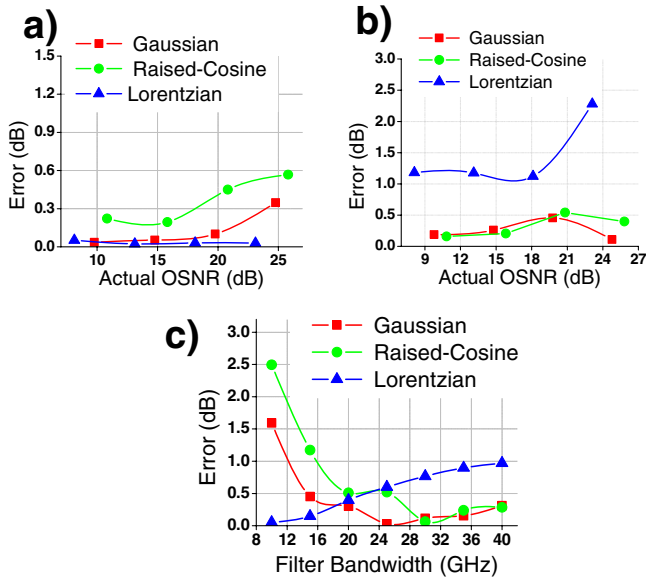
Fig. 3. (a) Simulated OSNR measurement error versus actual OSNR for single channel 100 Gbit/s PM-QPSK using Gaussian, raised-cosine, and Lorentzian filters. (b) Simulated OSNR measurement error versus actual OSNR for WDM 100 Gbit/s PM-QPSK using Gaussian, raised-cosine, and Lorentzian filters. (c) Simulated OSNR measurement error versus filter bandwidth for WDM 100 Gbit/s PM-QPSK using Gaussian, raised-cosine, and Lorentzian filters.
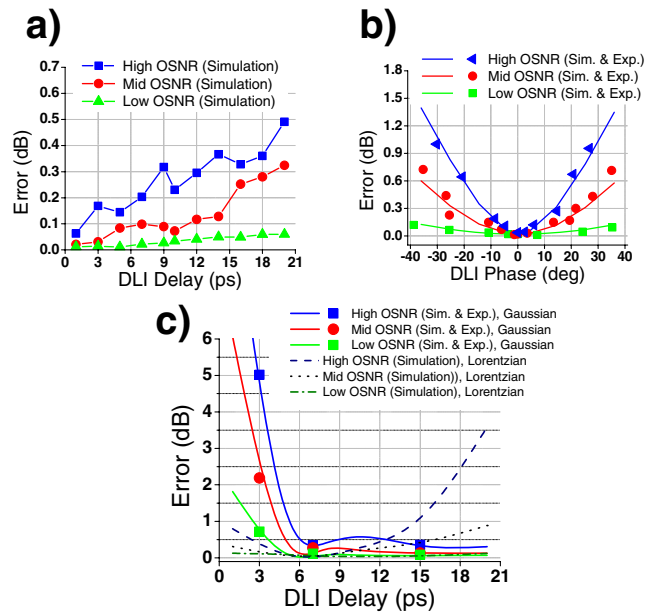
Fig. 4. (a) Simulated measurement error versus DLI delay for low (10 dB), medium (15 dB), and high (20 dB) OSNR, 100 Gbit/s PM-QPSK. (b) Measurement error versus DLI phase, simulation, and experimental results for low (10 dB), medium (15 dB), and high (20 dB) OSNR, 100 Gbit/s PM-QPSK. (c) Combination of phase-instability and measurement error versus DLI delay, simulation and experimental results for low, medium, and high OSNR, 100 Gbit/s PM-QPSK.
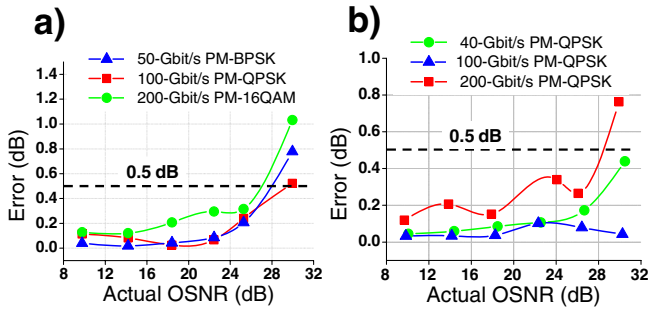
Fig. 5. (a) Measurement error versus actual OSNR for different modulation formats at the baud rate of 25-Gbaud. (b) Measurement error versus actual OSNR for different baud rates and the same modulation format PM-QPSK.

tuned accurately to the center of that channel. The filter bandwidth cannot be significantly wider than the effective bandwidth of each channel in order to minimize the negative effects of the leaked neighboring channels in the WDM systems [9]. Alternately, a very small narrow-band filter can lower the coherence difference between the signal and noise and consequently increase the error. Second, the shape of the filter's spectrum impacts the OSNR measurement error. For example, although the Lorentzian filter had better performance for single-channel OSNR monitoring, the Gaussian filter had significantly greater accuracy for the WDM system. Third, the trade-off in choosing the DLI delay value occurred because smaller delays can increase the accuracy of the OSNR monitor, but they are more sensitive to fluctuations in the phase of the DLI.

Figures 5 and 6 illustrate the accuracy of the DLI-based OSNR monitoring system for different modulation formats, different baud rate for PM-QPSK signals, and a four-channel WDM system with a 50-GHz ITU grid. The calibration process needs to be done for each modulation format and each baud rate separately. Here, because we monitored multiple 50-GHz-spaced channels at 25-Gbaud, a Gaussian filter with ~35 GHz bandwidth, and a DLI with 7-ps delay performed OSNR monitoring with the highest possible accuracy. For the data-format transparency and bit-rate-tunability experiments, we used the same monitor components except, for the 10- and 50-Gbaud PM-QPSK, we used filters with 25- and 100-GHz bandwidths, respectively.

Figure 5(a) shows a single channel at 1550.12 nm modulated using BPSK, QPSK, and 16-QAM formats at

25-Gbaud. The results showed that the OSNR monitor can perform accurately independent of the data format, and the error of the OSNR measurements remained less than the 0.5 dB threshold up to 26 dB actual OSNR for various modulation formats with the same baud rate. Figure 5(b) shows the measurement accuracy for the PM-QPSK signal with various baud rates (10, 25, and 50-Gbaud). Although the DLI delay was fixed at 7-ps, the filter bandwidth was changed accordingly for each baud rate. Similarly, <0.5 dB measurement error was observed for various bit rates for signals with <26 dB actual OSNR.

Figure 6(a) shows the measured OSNR versus the actual OSNR for four WDM channels at the 50-GHz ITU grid. For OSNR values of <26 dB, the OSNR monitor achieved <0.5 dB accuracy for all channels in the presence of neighboring channels. The similarity of the depicted curves for different WDM channels verified the wavelength independency of the system. Figure 6(b) shows the measurement error versus actual OSNR of channel 2 (1550.12 nm) while the OSNR of the adjacent channels are fixed at 15-dB (low-OSNR) and 20-dB (high-OSNR).

Fig. 6. (a) Measured versus actual OSNR for four 25-Gbaud PM-QPSK WDM channels and average error. (b) Measurement error versus actual OSNR for channel 2 (1550.12 nm) when other adjacent channels are either at high-or low-OSNR.

References

1. D. C. Kilper, R. Bach, D. J. Blumenthal, D. Einstein, T. Landolsi, L. Ostar, M. Preiss, and A. E. Willner, J. Lightwave Technol. **22**, 294 (2004).
2. E. Flood, W. H. Guo, D. Reid, M. Lynch, A. L. Bradley, L. P. Barry, and J. F. Donegan, Opt. Express **14**, 58 (2010).
3. M. D. Pelusi, A. Fu, and B. J. Eggleton, Opt. Express **18**, 9435 (2010).
4. W. Chen, R. S. Tucker, X. Yi, W. Shieh, and J. S. Evans, IEEE Photon. Technol. Lett. **17**, 2484 (2005).
5. K. Xu, H. K. Tsang, G. K. P. Lei, Y. M. Chen, L. Wang, Z. Cheng, X. Chen, and C. Shu, IEEE Photon. J. **3**, 968 (2011).
6. C. P. Lai, J.-Y. Yang, A. S. Garg, M. S. Wang, M. R. Chitgarha, A. E. Willner, and K. Bergman, Opt. Express **19**, 14871 (2011).
7. J. H. Lee, H. Y. Choi, S. K. Shin, and Y. C. Chung, J. Lightwave Technol. **24**, 4162 (2006).
8. C. Xie, D. C. Kilper, L. Moller, and R. Ryf, J. Lightwave Technol. **25**, 177 (2007).
9. M. Skold, B.-E. Olsson, H. Sunnerud, and M. Karlsson, *Optical Fiber Communication Conference (OFC)* (2007), paper OThH3.
10. L.-S. Yan, X. S. Yao, Y. Shi, and A. E. Willner, J. Lightwave Technol. **23**, 3290 (2005).
11. G.-W. Lu, M.-H. Cheung, L.-K. Chen, and C.-K. Chan, Opt. Express **14**, 58 (2006).
12. Y. K. Lizé, J. Y. Yang, L. Christen, X. Wu, S. Nuccio, T. Wu, A. E. Willner, R. Kashyap, and F. Séguin, *Optical Fiber Communication Conference (OFC)* (2007), paper OThN2.
13. X. Liu, Y.-H. Kao, S. Chandrasekhar, I. Kang, S. Cabot, and L. L. Buhl, IEEE Photon. Technol. Lett. **19**, 1172 (2007).
14. J. M. Oh, M. Brodsky, L. E. Nelson, G. Cadena, and M. D. Feuer, Opt. Lett. **33**, 2065 (2008).
15. E. Flood, W. H. Guo, D. Reid, M. Lynch, A. L. Bradley, L. P. Barry, and J. F. Donegan, *European Conference on Optical Communication (ECOC)* (2010), paper Th.9.C.6.
16. M. R. Chitgarha, S. Khaleghi, W. Daab, M. Ziyadi, A. Mohajerin-Ariaei, D. Rogawski, M. Tur, J. D. Touch, V. Vusirikala, W. Zhao, and A. E. Willner, *Optical Fiber Communication Conference (OFC)* (2013), paper OTh3B.